A New Discontinuous Conduction Mode in a Transformer Coupled High Gain DC-DC Converter

Kartikeya JP Veeramraju*, Jacob Eisen†, Joshua L Rovey†, Jonathan W Kimball*
*Department of Electrical and Computer Engineering, Missouri University of Science and Technology, Rolla, MO USA
{kvkhh, kimballjw}@mst.edu
†Department of Aerospace Engineering, University of Illinois Urbana-Champaign, Urbana, IL USA
{eisen3, rovey}@illinois.edu

2022 IEEE Applied Power Electronics Conference and Exposition (APEC) | 978-1-6654-0688-8/22/$31.00 ©2022 IEEE | DOI: 10.1109/APEC43599.2022.9773417

***Abstract*—Electrospray space propulsion thrusters often employ transformer coupled high gain dc-dc converters. These thrusters have a unique load resistance profile that can vary dramatically during operation. Transformer coupled high gain dc-dc converters working in very low power modes can enter a unique discontinuous conduction mode (DCM) caused by a coupling effect between the boost and magnetization inductors in the converter. The transformer magnetization current prevents the boost inductors from discharging properly, which causes premature loss of boost action and higher than expected boost inductor voltages. This mechanism generates abnormally high voltages on the converter's output side, leading to converter and thruster failure. Parameter sweep simulations show that once the converter's load resistance range is known, this DCM can be prevented or have its effects minimized by increasing the transformer magnetization inductance, the boost inductance, and the converter operating frequency. The voltage waveform across the transformer's primary winding can be actively monitored for the presence of this DCM, and the converter's operating frequency and duty cycle can be dynamically modified to ensure the converter remains in continuous conduction mode (CCM).**

***Index Terms*—aerospace propulsion, electric thrusters, space propulsion, electric rocket engines, high-voltage converter, lightweight high-voltage power converters**

I. Introduction

High gain dc-dc converters are employed to power some electric space propulsion engines, where the available low voltage power source (such as batteries and solar cells) cannot directly meet the high voltage operating requirement. This article builds on transformer-coupled high voltage converters that employ voltage multiplier cells for use with electric space propulsion thrusters, as documented in [1]–[4].

The power converter (intended for use with electrospray thrusters) is a transformer-coupled high gain dc-dc converter [2]. The main design requirements of this converter are high voltage gain, small size, and high efficiency to ensure integrability and low power consumption. The converter should also maintain its output voltage during load resistance changes for a fixed duty cycle and switching frequency. While performing PLECS® circuit simulations to prepare for electrospray applications of this converter, the converter's output voltage was observed to have an unexpected dependence on thruster impedance [5] as shown in Figure 1. This research investigates the mechanism behind this anomalous output voltage increase at high output impedances, and a new kind of discontinuous conduction mode (DCM) is described. The voltage anomaly is problematic as the thruster has a widely varying load profile due to variable emission modes.

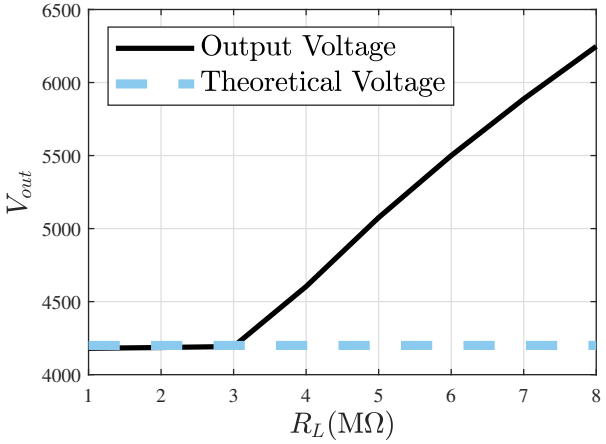

Fig. 1: Anomalous voltage behavior in the converter. Operation conditions: 100 kHz, $L = 400\,\mu\mathrm{H}$, $Lm = 1.5\,\mathrm{mH}$

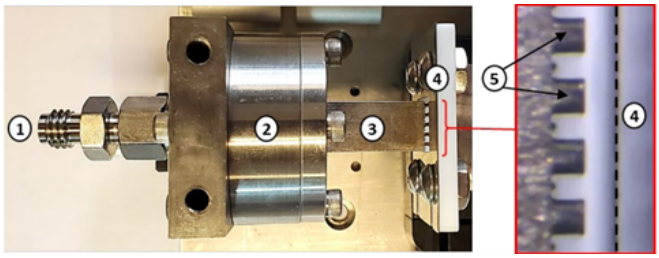

Fig. 2: MEPS thruster at UIUC's Electric Propulsion Laboratory. Reprinted from [6] with permission. (1) Propellant inlet, (2) Propellant manifold, (3) Emitter array, (4) Extractor, (5) Emitter tips.

Section II introduces the electrospray thruster and provides a short discussion on its relevance in the context of the converter. Section III introduces the converter topology, and Section IV presents the theory behind the observed DCM. Section V presents parametric sweep results for relevant parameters, with the intent of exploring the dependencies of this voltage anomaly. Finally, Section VI provides passive and active

mitigation strategies to prevent the occurrence of this anomaly or reduce its effects.

II. Electrospray Thruster Load Characteristics

Electrospray thrusters are a class of low-thrust electric space propulsion engines which use an ionic liquid as propellant. The Monopropellant-Electrospray Propulsion System (MEPS) (developed by Froberg Aerospace, LLC and the University of Illinois Urbana-Champaign) is an electrospray thruster of the capillary type, in which the ionic liquid is fed at a low flow rate through many parallel microchannels [6]. These emitter microchannels have exits facing an extractor electrode. When a sufficient voltage is applied between the emitters and extractor, the ionic liquid at each emitter tip is pulled into the shape of a Taylor cone, emitting the ionic liquid as a current in the form of charged droplets or ions. The emitted propellant then passes through gaps in the extractor plate. A diagram of the MEPS thruster is shown in Figure 2.

These thrusters are often characterized with a current-voltage (IV) curve that demonstrates the current emitted as a function of the emitter-extractor voltage applied. An example IV curve is presented in Figure 3. Since the slope of this curve changes, the thruster's electrical impedance also changes according to Ohm's law. One single static impedance value is not sufficient to describe the current-voltage relationship exhibited by electrospray thrusters.

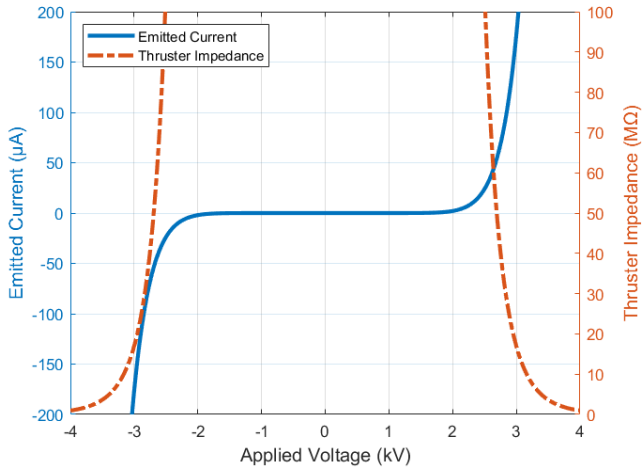

Fig. 3: IV Curve Example

The thruster's electrical impedance also changes over $time$. For example, during startup, there is a delay before propellant begins to spray from the emitters, as propellant takes time to travel from the reservoir to the emitter tips or orifices. During this time, the thruster's impedance is effectively infinite as no current flows. Even once propellant reaches the emitter tips or orifices, all emitters may not begin producing current at the same time; emitter geometry manufacturing tolerances may lead to differences in flow rate (and thus differences in emission start time) [6].

Transient arcing events are possible between the emitters and extractor [5], [7]. During these events, the thruster's impedance drops suddenly due to the high current flow. Prolonged arcing events can end nominal electrospray thruster operations.

An electrospray thruster's effective electrical impedance changes in both predictable and unpredictable ways during use. Any power processing unit (PPU) architecture designed to provide the high voltage necessary for electrospray operation must handle these varying electrical load characteristics. As Figure 1 shows, the power converter described in this paper does not meet that criteria, as its output voltage rises sharply for high output load resistance values. Additional considerations must be made to successfully apply the converter to electrospray thrusters with a high electrical impedance.

III. Power Converter Topology

The high gain dc-dc converter consists of three stages: a Two-Phase Interleaved (TPI) boost stage, followed by a High-Frequency Transformer (HFT) stage, and finally a Cockcroft Walton Voltage Multiplier (CWVM) stage. The three stages have a combined ideal theoretical gain of

$$\frac{V_o}{V_{in}} = \frac{2N_{CW}}{(1-d)}\frac{N_2}{N_1} \tag{1}$$

where N_{CW} is the number of CWVM stages, N_2 and N_1 are the number of secondary and primary turns, respectively, V_{in} is the input voltage, and d is the duty cycle applied to the TPI stage. A schematic of the power converter is shown in Figure 4.

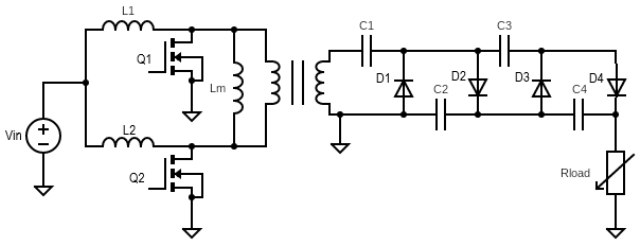

Fig. 4: Transformer coupled high gain dc-dc converter

The MOSFETs Q1 and Q2 are switched in anti-phase at a minimum duty cycle of at least 50% to prevent inductor voltage spiking. When the converter operates in continuous conduction mode (CCM), the inductor currents (I_{L1} and $-I_{L2}$), the magnetization inductor current (I_{Lm}), the transformer primary's modified square wave (MSW) waveform, and the CWVM input current ($i_{se}(t)$) are as shown in Figure 5. The MSW waveform's peak voltage value, represented as $v_{MSW}(t)$ in Figure 5, appears to agree with the theoretical voltage value given by $V_{in}/(1-d)$ (which is 50 V for the parameters shown in Figure 5). The CWVM capacitors charge throughout the application of the MSW signal as shown by the transformer's secondary side current ($i_{se}(t)$) plot. For ease of

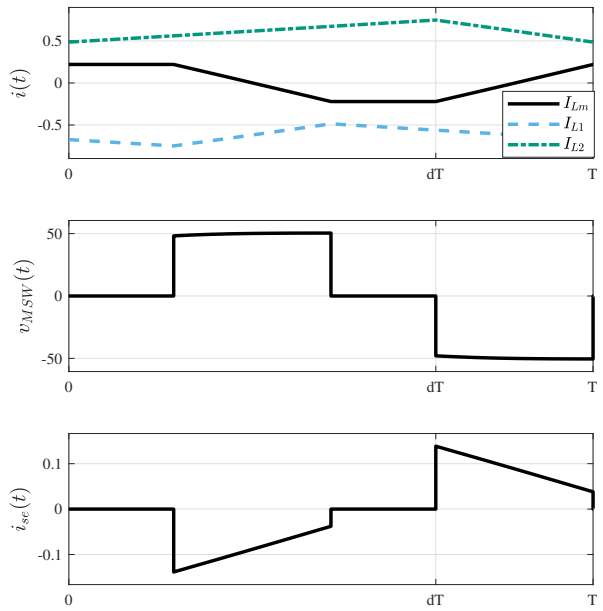

Fig. 5: Converter operating in CCM at L = 400 µH, L_m = 340 µH, $d = 0.7$, $V_{in} = 15\,\mathrm{V}$ and $R_L = 1\,\mathrm{M\Omega}$

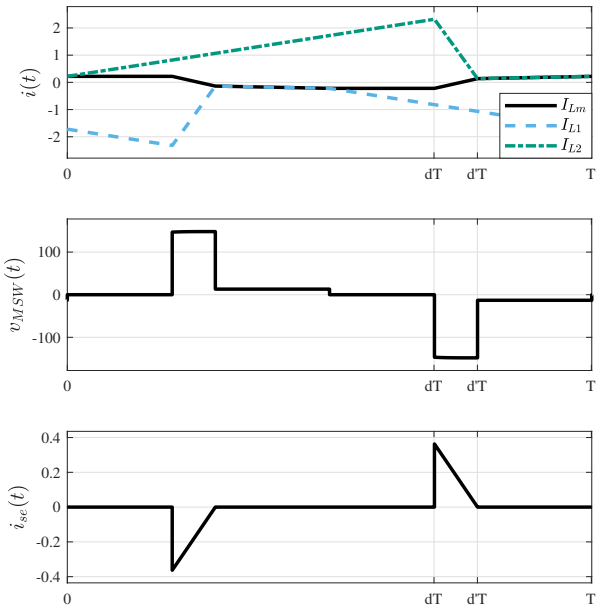

Fig. 6: Converter operating in DCM at L = 50 µH, L_m = 340 µH, $d = 0.7$, $V_{in} = 15\,\mathrm{V}$ and $R_L = 5\,\mathrm{M\Omega}$

visualization in subsequent sections, the L_1 and L_2 currents, I_{L1} and $-I_{L2}$ respectively (as per transformer's input), are plotted over the magnetization inductance current plot (I_{Lm}).

The converter is designed for a maximum power of 10 W, an input voltage of 15 V and a target output voltage of 4.2 kV. The converter is designed using an HFT ratio of 1:7 and six cascaded CWVM stages.

IV. Discontinuous Conduction Mode

The steady state output voltage plot in Figure 1 is a PLECS® simulation demonstrating that the converter obeys the theoretical voltage gain expression given by (1) for an output impedance of up to 3 MΩ, after which its output voltage deviates sharply from that expected relationship. This can damage the CWVM stage capacitors, diodes, and the application load. This section describes an investigation of the reasons behind this sharp increase in voltage, and the mathematical equations governing the behavior are presented.

A. Load Sweep Effects and Duty Squeezing

The main reason for the onset of this anomalous voltage mechanism is the rapid charging of the CWVM stage capacitors, as shown in Figure 6. When the CWVM capacitors are done charging, the boost inductor current drops to the magnetizing inductor current level—that is, at this point, the boost inductor current ($i_{L_1}(t)$, or $i_{L_2}(t)$) is equal to the magnetizing inductor current ($i_{Lm}(t)$). When either of the boost inductor currents are equal to the magnetizing inductor current, the voltages across the HFT magnetizing inductor and the boost inductor are distributed according to the magnetization inductance and boost inductance ratio. Therefore, the boost inductor voltage during this loss of boost action is given by

$$V_L = \frac{L}{L + L_m} V_{in} \tag{2}$$

where L is the boost inductance and L_m is the HFT magnetization inductance. When operating in CCM, the TPI stage output voltage is typically given by $V_{in}/(1-d)$ (which is equivalent to the boost inductor voltage). The relationship shown in (2) therefore demonstrates a decrease from the nominal TPI stage output voltage, which causes a complete loss of boost action when the boost inductor current equals the magnetization current. Therefore, under steady-state operation, the inductor loses its energy at a higher voltage due to the volt-second balance equation given by

$$dV_{in} + (d' - d)V_{MSWpk} + (1 - d')\frac{L}{L + L_m}V_{in} = 0 \tag{3}$$

where V_{MSWpk} (referred to as $v_{MSW}(t)$ in Figure 6) is the peak voltage of the MSW across the HFT primary, d is the duty cycle impressed by the switching signal, and d' is the period-relative time at which the boost inductor discharge is prematurely ended. If the converter operates in CCM, the MSW peak will extend for an interval of $1 - d$. When the converter operates in this unique DCM, the MSW peak only has a window of $d' - d$ before the boost inductor current crashes into the magnetizing inductor current. This shortened boost inductor discharge results in a narrower MSW peak, and this phenomenon is known as "duty squeezing." As the boost inductor voltage cannot rise above the value of the input voltage during DCM as described in (2), the MSW waveform

has to rise more than the theoretically expected value prior to the DCM operation (i.e. the $d' - d$ window) and causes the deviation from the conventional boost converter's output voltage relationship. When impressed across the CWVM stage via the transformer, this sharply increasing MSW voltage causes a drastically higher voltage than what would have normally been expected. CCM operation is ensured when $d' = 1$ (which can be verified from (3)) and DCM operation occurs when $d' < 1$.

B. Inductor Currents

The minimum boost inductor current (I_{min}) during nominal (CCM) converter operation is given by

$$I_{min} = \frac{\langle I_{in} \rangle}{2} - \frac{V_{in}}{2L} dT \tag{4}$$

where $\langle I_{in} \rangle$ is the average input current approximated by conservation of energy in ideal conditions and T is the switching period. The Fourier expansion for the MSW waveform (referred to as $v_{MSW}(t)$ in this article) is given by

$$v_{MSW}(t) = \sum_{k=1}^{\infty} a_k \cos(k\omega_0 t) + b_k \sin(k\omega_0 t) \tag{5}$$

$$\begin{aligned} a_k = \frac{V_{in}}{(D-1)k\pi} \Big[& \sin(k\pi) - \sin(2k\pi) \\ & + \sin((1-2D)k\pi) + \sin(2Dk\pi) \Big] \end{aligned} \tag{6}$$

$$\begin{aligned} b_k = \frac{V_{in}}{(D-1)k\pi} \Big[& -\cos(k\pi) + \cos(2k\pi) \\ & + \cos((1-2D)k\pi) - \cos(2Dk\pi) \Big] \end{aligned} \tag{7}$$

where a_k and b_k are the k^{th} harmonic coefficients of the Fourier series and $\omega_0 = 2\pi f_{sw}$. Therefore, the values of the magnetization current are approximated for MSW excitation in CCM by the superposition of the various phasors given by

$$\vec{I}_{Lm_k} = \frac{a_k \angle -90^\circ}{\sqrt{2}(k\omega_0 L_m)} + \frac{b_k \angle 0^\circ}{\sqrt{2}(k\omega_0 L_m)} \tag{8}$$

$$\vec{I}_{Lm} = \sum_{k=1}^{\infty} \vec{I}_{Lm_k} \tag{9}$$

The validation for (9) is given in Figure 7.

Therefore, a design rule for ensuring CCM for a given load resistance is written as

$$I_{min} > \max(\vec{I}_{Lm}) \tag{10}$$

V. Simulation Results for Parametric Sweeps

As discussed in Section IV, when providing low power, the converter's operating mode (CCM or DCM) depends on the boost inductor current's minimum value, the amplitude of the magnetizing inductor current, and the switching frequency. Therefore, for a particular load configuration, it is essential to understand how circuit parameters affect the CCM/DCM behavior of the PPU and its ability to maintain a constant output voltage for different load conditions. In this section, results for three parameter sweep simulations are presented. The first parameter sweep is the boost inductance value sweep. Next, the magnetization inductance value sweep is presented. Finally, a sweep of the converter's operating frequency is shown. The number of CWVM stages was chosen to be six for all sweeps, and the transformer turns ratio was fixed at 1:7. The input voltage and duty values were chosen to be 15 V and 0.7, respectively.

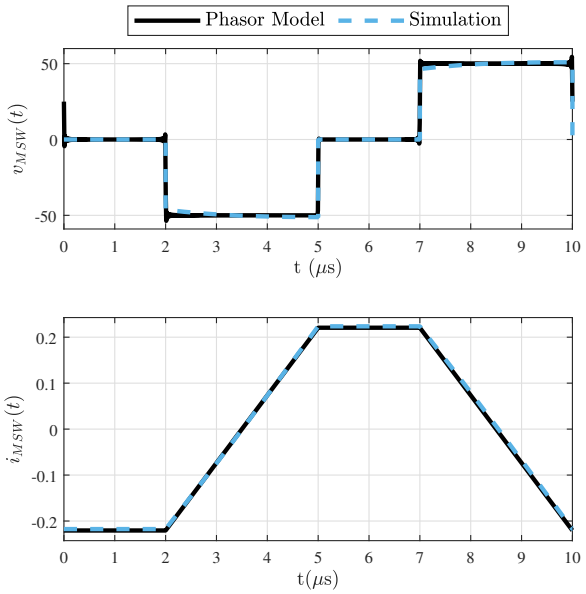

Fig. 7: Validation of magnetization inductor current's phasor model (Eqn. (9)) by comparison with simulation. Input parameters are $L_m = 340\,\mu\text{H}$, $d = 0.7$, $V_{in} = 15\,\text{V}$ and $f_{sw} = 100\,\text{kHz}$

As the effects of this DCM can damage hardware, it is important to study these DCM effects in a purely computational setting. Therefore all results presented in this section are simulation-based. A model of the converter is constructed in PLECS® blockset environment available in Simulink® and the test scripts and plots are automated in MATLAB®.

A. Boost Inductance Sweep

The boost inductance is swept through the values presented in Table I. The design rule shown in (10) is obeyed for some values of boost inductance and violated for others to show how violating this condition affects the circuit. The load resistance is varied from $1\,\text{M}\Omega$ to $8\,\text{M}\Omega$ to show the effect of boost inductance choice at different load resistance values. In the first subplot of Figure 8, the minimum boost inductor current is plotted for each boost inductance and output load resistance value. Here, the dashed line represents the maximum magnetization inductor current. In the second subplot, the steady-state output voltage of the PPU is also plotted for each case.

TABLE I: Parameters for Boost Inductance Sweep

Parameter	Value
f_{sw}	100 kHz
C	0.1 µF
esr for C	100 mΩ
L	200 µH - 1.2 mH
esr for L	1 mΩ
Lm	1.5 mH
R_L	1 MΩ - 8 MΩ
V_{in}	15 V
d	70%
N_1/N_2	1/7

TABLE II: Parameters for Magnetization Inductance Sweep

Parameter	Value
f_{sw}	100 kHz
C	0.1 µF
esr for C	100 mΩ
L	400 µH
esr for L	1 mΩ
Lm	200 µH - 1.2 mH
R_L	1 MΩ - 8 MΩ
V_{in}	15 V
d	70%
N_1/N_2	1/7

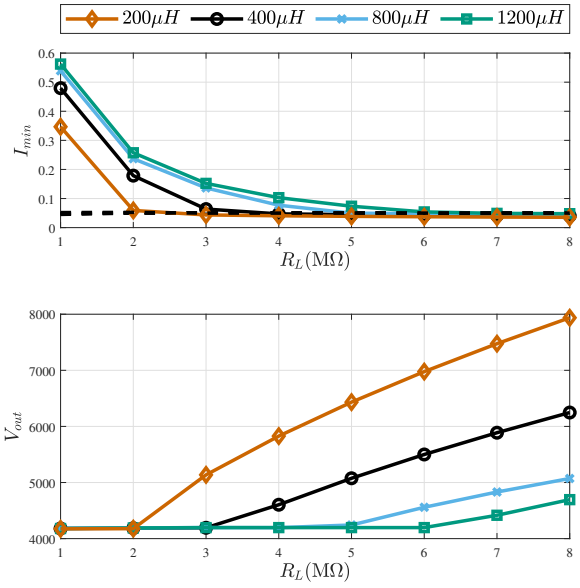

Fig. 8: Boost inductance parametric sweep plot

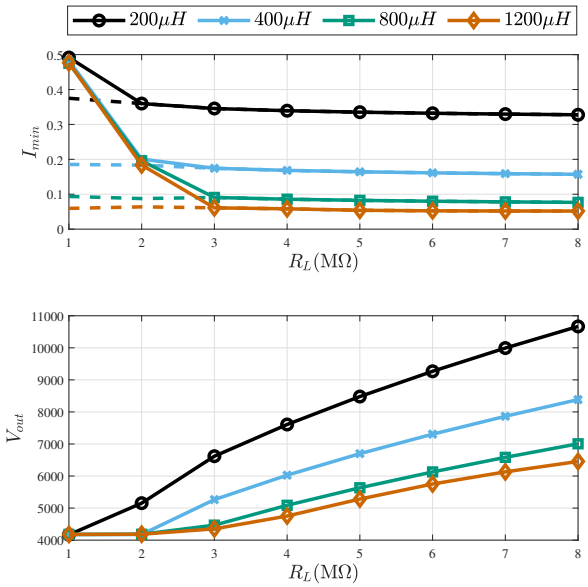

Fig. 9: Magnetization inductance parametric sweep plot.

The second subplot of Figure 8 shows that for higher values of boost inductance, the onset of DCM is shifted to the right. This allows for a larger tolerance on the allowed electrospray thruster electrical impedance. When operating in DCM, the output voltage for a given load resistance is reduced with increasing boost inductance values. The first subplot of Figure 8 shows that this decrease in severity of the anomalous voltage is because higher boost inductance values move the minimum boost inductor current away from the maximum magnetization inductor current. This provides a greater buffer on the design rule shown in (10).

B. Magnetization Inductance Sweep

The magnetization inductance is swept for a fixed value of boost inductance as described by the parameters in Table II.

The results of the L_m parameter sweep simulations are shown in Figure 9. The first subplot shows the minimum values of boost inductor current at steady state, and the same-colored dashed line is the corresponding boundary set by $\max(I_{Lm})$. The second subplot depicts the output voltage at each load resistance value, swept over several magnetization inductance values. If the converter were ideal and in CCM, each of the output voltage traces would be horizontal and lay on top of each other. It is clear, then, that most of the output voltage plot is in the DCM regime. Increasing the value of magnetization inductance also increases the load resistance allowed while remaining in CCM. Additionally, higher magnetization inductance values decrease the voltage overshoot when in DCM.

C. Switching Frequency Sweep

The switching frequency sweep was performed using the parameters in Table III. The results of this sweep are shown in Figure 10. The process of increasing frequency achieves two essential things, namely:

1) Reducing the boost inductor current ripple and increasing the minimum boost inductor current as described by (4)
2) Increasing the magnetizing inductor reactance, which leads to lower magnetizing current magnitudes as described in (9)

TABLE III: Parameters for Switching Frequency Sweep

Parameter	Value
f_{sw}	100 kHz - 1.2 MHz
C	0.1 µF
esr for C	100 mΩ
L	200 µH
esr for L	1 mΩ
Lm	400 µH
R_L	1 MΩ - 8 MΩ
V_{in}	15 V
d	70%
N_1/N_2	1/7

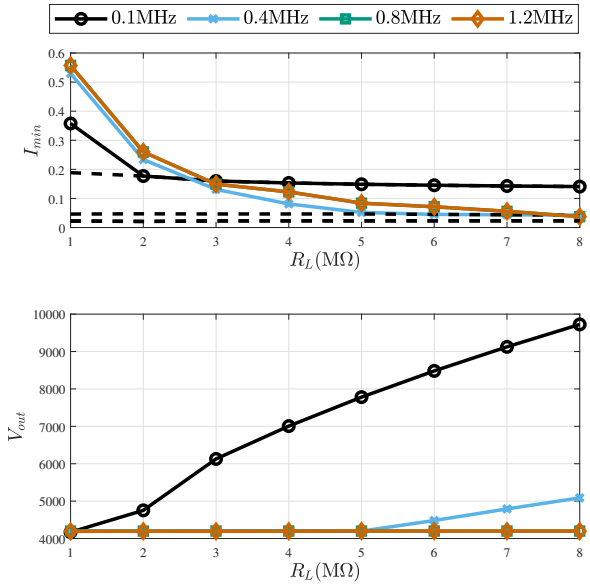

Fig. 10: Frequency sweep effects

Therefore, a frequency increase leads to improved margins for the design rule described by (10) and shifts the DCM onset to higher load resistance values. The usefulness of frequency increases will be described in more detail in Section VI.

In the context of the load specifications and voltage ranges described for the PPU and thruster application, Figure 10 shows that the process of shifting to higher switching frequencies successfully maintains the output voltage at the theoretical values described in (1) for higher load resistance ranges at switching frequencies starting at around 0.8 MHz

VI. Mitigation of DCM Effects

The condition for CCM expressed in (10) can be maintained in a number of ways. Carefully selecting values for L and L_m for all load and duty ranges during the design phase can ensure the converter remains in CCM during nominal operation. A nominal value for f_{sw} can also be selected during the design phase—increasing the nominal operating frequency raises the minimum boost inductor current as seen in (4), improving the margins for (10). Yet another passive solution is to place a resistor in parallel with the too-high intended load resistance

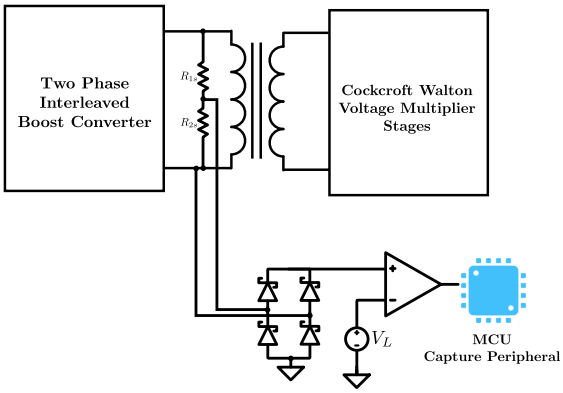

Fig. 11: MSW duty sensing based DCM detection

(the electrospray thruster in this case) to lower the output electrical impedance seen by the converter. Though this can result in a significant efficiency loss, this may be an acceptable solution for an electrospray thruster because it also resolves the startup problem of infinite thruster electrical impedance discussed in Section II.

In addition to these static or passive methods of maintaining CCM, there are several possible active control methods. The circuit can be monitored for DCM behavior, and corrections to circuit parameters can be made via feedback. The output voltage is a good indicator of DCM behavior—if it is higher in magnitude than analytically predicted by CCM transfer functions, this strongly suggests the converter is in DCM. However, in practice, measuring the output voltage and providing appropriate feedback is a slow process [8], [9], during which the higher-than-expected voltages may exceed component limits and damage the converter. Another possible active control method is monitoring the boost inductor current for the "shaving" effect seen in Figure 6.

The active control scheme with the most promise may be to monitor the primary MSW. A higher-than-predicted maximum voltage on the primary MSW would indicate DCM operation. Its duty cycle should be the complement of the duty cycle applied to the MOSFETs. If the MSW's duty cycle is lower than $(1 - d_{CMD})$ (where d_{CMD} is the commanded duty value and d'_{DCM} is the squeezed duty under DCM), then this indicates the duty squeezing effect discussed in Section IV. This could be detected via the use of a comparator, with a threshold voltage set slightly lower than what is found using (2) after accounting for any appropriate scaling that may be necessary. A possible MSW duty detection scheme is shown in Figure 11. In this example, the primary MSW is scaled down through a voltage divider, rectified, and then connected to the comparator and capture peripheral for processing. The corresponding waveforms are shown in Figure 12. The MSW voltage is converted to digital values and the duty cycle can be calculated using the known period. This detection method is strong when measuring either the amplitude or duty cycle because DCM is observable within a single period. This fact, combined with the observed waveform's early position in

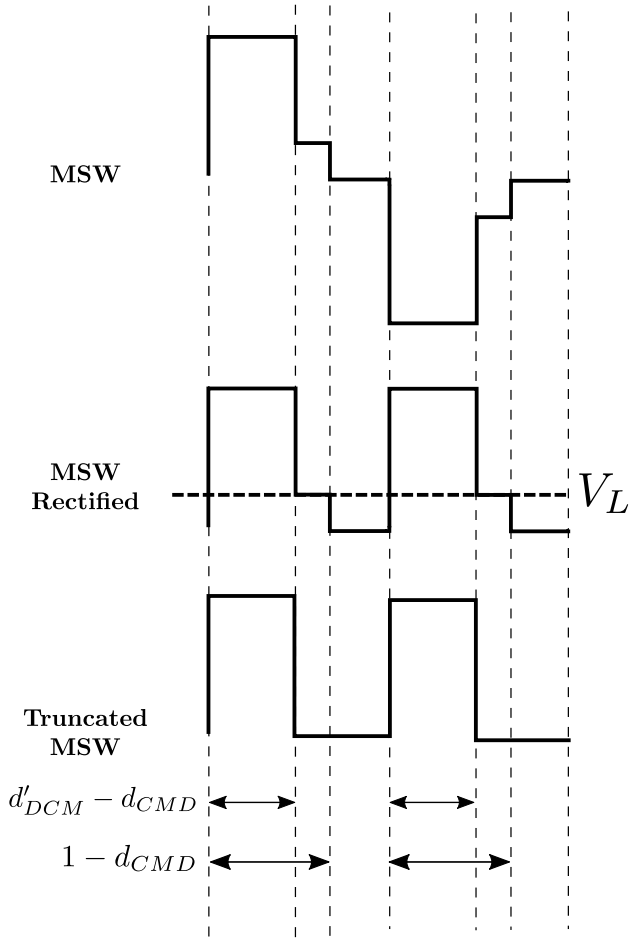

Fig. 12: MSW based DCM detection waveforms

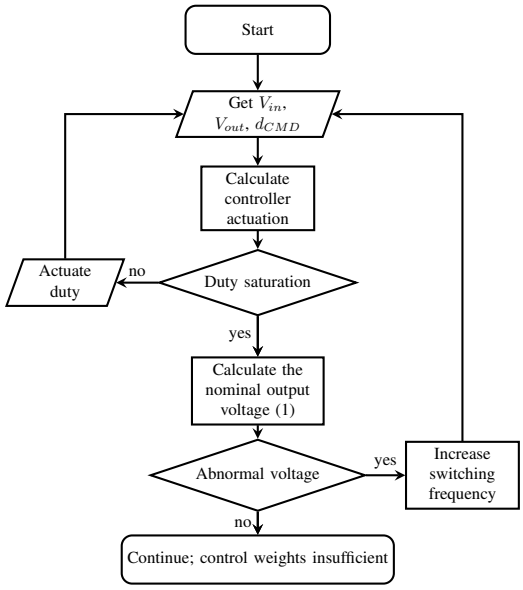

Fig. 13: Output voltage sensing based dynamic DCM diagnostics and correction scheme

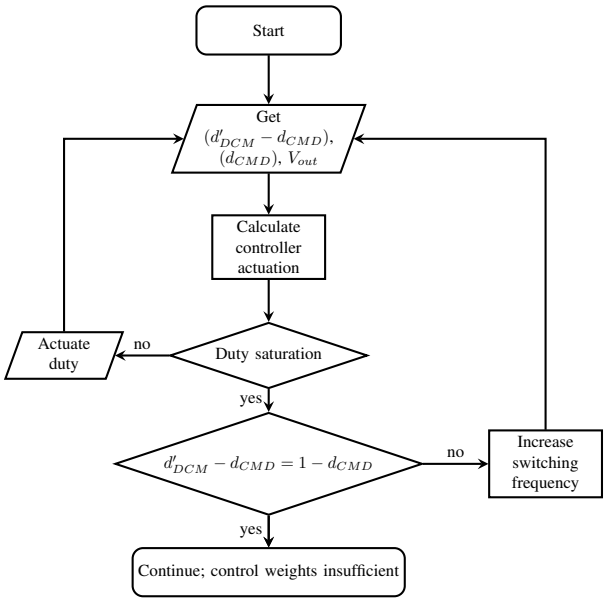

Fig. 14: MSW duty sensing based dynamic DCM diagnostics and correction scheme

the circuit, should make the feedback process faster than the output voltage detection scheme. Isolation is also less of a concern when using primary MSW detection because the voltages are lower at this location in the circuit.

If an active control system detects DCM, then the converter's switching frequency can be increased until DCM is no longer detected. Figure 13 shows how this feedback system would work for the output voltage detection method, and Figure 14 shows how this would work for the transformer primary MSW duty detection method. There are limits on the operating frequency in a practical converter, such as transformer resonance and transformer core choice. Additionally, regardless of mitigation method, circuit component ratings should account for the possibility of this DCM condition. For example, when this converter is applied to an electrospray thruster, the expected range of thruster electrical impedance should be considered when choosing CWVM capacitor voltage ratings.

VII. Conclusions

This work investigates a DCM that arises in low-power high voltage dc-dc converters. This DCM is caused by a complex coupling mechanism between the boost and magnetization inductances. The voltage deviation results from the low currents caused by the high output load resistance and the fast charging mechanism of the CWVM stage capacitors. This DCM is not a result of the boost inductor currents reaching zero, but is due to the boost inductor currents reaching the levels of the HFT magnetization inductor current (something that does not typically occur in *high*-power dc-dc converters). Parametric sweeps are performed to explore their effects on the DCM. These sweeps inform design recommendations for passively

and actively curbing the onset of DCM. A more robust scheme for detecting and curbing this unique DCM will be investigated in future work, and hardware results are being pursued.

ACKNOWLEDGMENT

The authors thank Corey Rhodes, Luis Pinero, and Thomas Liu from NASA Glenn Research Center for their time, expertise, and insight. This work was partially supported by the NASA SmallSat Technology Partnerships program, grant number 80NSSC20M0089.

REFERENCES

[1] F. Mier-Hicks and P. C. Lozano, "Spacecraft-charging characteristics induced by the operation of electrospray thrusters," *Journal of Propulsion and Power*, vol. 33, no. 2, pp. 456–467, 2017. [Online]. Available: https://doi.org/10.2514/1.B36292

[2] K. J. Prasad Veeramraju and J. W. Kimball, "An improved power processing unit for multi-mode monopropellant electrospray thrusters for satellite propulsion systems," in *2019 IEEE Energy Conversion Congress and Exposition (ECCE)*, 2019, pp. 1302–1309.

[3] B. P. R. Baddipadiga, V. A. K. Prabhala, and M. Ferdowsi, "A family of high-voltage-gain dc–dc converters based on a generalized structure," *IEEE Transactions on Power Electronics*, vol. 33, no. 10, pp. 8399–8411, 2018.

[4] Y. He, M. Woolston, and D. Perreault, "Design and implementation of a lightweight high-voltage power converter for electro-aerodynamic propulsion," in *2017 IEEE 18th Workshop on Control and Modeling for Power Electronics (COMPEL)*, 2017, pp. 1–9.

[5] J. G. Eisen, B. C. Cline, S. P. Berg, and J. L. Rovey, "Power processing unit and feed system development for a multimode spacecraft propulsion system," in *AIAA Propulsion and Energy 2021 Forum*, 2021.

[6] C. T. Lyne, J. Rovey, and S. P. Berg, *Monopropellant-Electrospray Multimode Thruster Testing Results: Electrospray Mode*. [Online]. Available: https://arc.aiaa.org/doi/abs/10.2514/6.2021-3439

[7] F. Mier-Hicks, "Characterization on a magnetically levitated testbed for electrospray propulsion systems," 10 2014.

[8] A. Lamantia, P. Maranesi, and L. Radrizzani, "Small-signal model of the cockcroft-walton voltage multiplier," *IEEE Transactions on Power Electronics*, vol. 9, no. 1, pp. 18–25, Jan 1994.

[9] K. J. P. Veeramraju, "Design and development of power processing units for applications in electrically-propelled satellite systems," Master's thesis, Missouri University of Science and Technology, 2020, aAI27735442.